HHS Public Access

Author manuscript

J Physiol. Author manuscript; available in PMC 2023 January 01.

Published in final edited form as:

J Physiol. 2022 January ; 600(1): 111–122. doi:10.1113/JP282438.

α2δ−2 is Required for Depolarization-Induced Suppression of Excitation in Purkinje Cells*

Kathleen A. Beeson[1,2], **Gary L. Westbrook**[3], **Eric Schnell**[2,4,**]

[1]Neuroscience Graduate Program, OHSU, Portland, OR, 97239

[2]Department of Anesthesiology and Perioperative Medicine, OHSU, Portland, OR, 97239

[3]Vollum Institute, OHSU, Portland, OR, 97239

[4]Operative Care Division, Portland VA Health Care System, Portland, OR, 97239

Abstract

α2δ proteins (*CACNA2D1–4*) are required for normal neurological function and contribute to membrane trafficking of voltage-gated calcium channels, through which calcium entry initiates numerous physiological processes. However, it remains unclear how α2δ proteins influence calcium-mediated signaling to control neuronal output. Using whole-cell recordings of mouse Purkinje cells, we show that α2δ−2 is required for functional coupling of postsynaptic voltage-dependent calcium entry with calcium-dependent effector mechanisms controlling two different outputs, depolarization-induced suppression of excitation and spike afterhyperpolarization. Our findings indicate an important role for α2δ−2 proteins in regulating functional postsynaptic calcium channel-coupling in neurons, providing new context for understanding the effects of α2δ mutations on neuronal circuit function and presenting additional potential avenues to manipulate α2δ-mediated signaling for therapeutic gain.

Graphical Abstract

*Preprint Publication: This manuscript was first published as a preprint on BioRxiv: Beeson KA, Westbrook GL, Schnell E (2021). α2δ−2 is Required for Depolarization-induced Suppression of Excitation in Purkinje cells. BioRxiv. https://doi.org/10.1101/2021.03.25.437080

**Eric Schnell, MD, PhD, schneler@ohsu.edu.

Author Contributions: KAB designed and performed research, analyzed and interpreted data, and wrote the original paper; GLW interpreted data, reviewed and edited paper; ES designed research, interpreted data, reviewed and edited paper. The experiments were performed in the labs of Drs. ES and GLW. All authors have approved of this manuscript, are accountable for this work, and qualify for authorship.

Competing Interest Statement: The authors declare no competing financial interests.

Institutional Ethics Committee Approval number: OHSU IACUC Protocol IP00001622

Research Governance: Dr. Peter Barr-Gillespie, Executive Vice President and Chief Research Officer, Oregon Health and Science University, gillespp@ohsu.edu, 503–494-2936

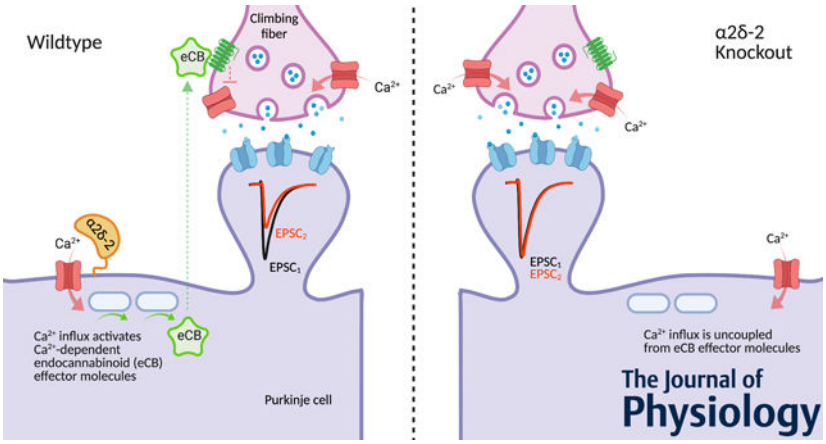

Schematic Depolarization-induced suppression of excitation (DSE) requires tight functional coupling of postsynaptic voltage-gated calcium channels (VGCCs) and endocannabinoid (eCB) effector systems, which generate eCBs in response to local calcium. Calcium influx produces eCBs in Purkinje cells, which retrogradely act on presynaptic climbing fiber terminals to acutely lower release probability, reducing subsequent excitatory postsynaptic currents (EPSCs). We find that deletion of α2δ−2, the only α2δ protein isoform expressed by Purkinje cells, functionally uncouples voltage-dependent calcium entry from eCB signaling in Purkinje cells, as DSE is blocked by increased intracellular calcium buffering in the α2δ−2 knockout. Created with BioRender.com

Keywords

α2δ−2 proteins; calcium channels; depolarization-induced suppression of excitation; nanodomains; endocannabinoid signaling; Purkinje cells

Introduction

Many intracellular signaling cascades are triggered by a common messenger: calcium entering via voltage-gated Ca^{2+} channels (VGCCs) on the plasma membrane. Specificity of Ca^{2+}-dependent signaling depends on close proximity of VGCCs to effectors in functional nanodomains, and this coupling is critical for neuronal function. For example, in Purkinje cells (PCs), depolarization-induced suppression of excitation (DSE) is initiated via Ca^{2+}-dependent endocannabinoid release (Kreitzer & Regehr, 2001b; Ohno-Shosaku et al., 2001; Brenowitz & Regehr, 2003; Brenowitz et al., 2006). Likewise, VGCC-K_{Ca} coupling generates spike afterhyperpolarization (AHP), ultimately setting firing frequency (Raman & Bean, 1999; Womack et al., 2004; Niday & Bean, 2021). Thus, molecules coupling VGCCs to effector-specific signaling critically contribute to transduction of neuronal outputs.

Auxiliary VGCC α2δ proteins (*CACNA2D1–4*) contribute to VGCC membrane trafficking (Dolphin & Lee, 2020), and may couple presynaptic VGCCs to molecules involved in vesicle exocytosis (Hoppa et al., 2012). However, there is little consensus about auxiliary postsynaptic functions of α2δ outside of these contexts, apart from developmental Ca^{2+}-independent roles (Eroglu et al., 2009; Kurshan et al., 2009). Indeed, postsynaptic

Ca^{2+} signals are tightly coupled to various effector molecules, such as K_{Ca} channels or Ca^{2+}-dependent enzymes involved in driving complex neurophysiological behaviors. Unfortunately, it is not known whether α2δ proteins mediate postsynaptic VGCC localization or effector coupling, as visualization of either endogenous α2δ proteins or VGCCs is severely limited in tissues. Furthermore, resolving molecular associations at the nanodomain scale (<100 nm) remains technically challenging. Thus, to test whether functional coupling of Ca^{2+}-dependent signaling is regulated by α2δ proteins, we used whole-cell electrophysiological recordings and internal Ca^{2+} buffering – tools that have been fundamental for the investigations of VGCC-coupling at presynaptic terminals.

In Purkinje cells (PCs), which exclusively express α2δ−2 (Lein et al., 2007; Beeson et al., 2020). deletion of α2δ−2 proteins (*CACNA2D2* KO) disrupted two disparate forms of postsynaptic voltage-dependent Ca^{2+} signaling as measured by whole-cell electrophysiological recordings. First, using intracellular Ca^{2+} buffering by EGTA in KO PCs, Ca^{2+}-dependent endocannabinoid (eCB) signaling became functionally uncoupled, blocking retrograde control of climbing fiber vesicle release. Conversely, reducing intracellular Ca^{2+} chelation in KO PCs restored the expression of Ca^{2+}-dependent eCB signaling, indicating the requirement of α2δ−2 proteins for postsynaptic Ca^{2+}-mediated nanoscale signaling. In support of these findings, we also found that α2δ−2 is required for a separate Ca^{2+}-dependent nanoscale signaling process, the K_{Ca}-mediated after-hyperpolarization (AHP). Taken together, our data demonstrate previously unappreciated roles for α2δ proteins in postsynaptic VGCC-effector coupling, and may shed light on mechanisms by which α2δ proteins contribute to neurological function.

Materials and Methods

Ethical Approval:

Cacna2d2 knockout mice (*Cacna2d2*^{tm1Svi}, MGI = 3055290; generously supplied by Drs. Sergey Ivanov and Lino Tessarollo) were obtained as cryopreserved sperm and re-derived via *in vitro* fertilization on a C57BL/6J background. Breeding mice were kept heterozygous, and genotyping was performed as previously described (Beeson et al., 2020). Food and water were available *ad libitum*. Mice were maintained in facilities fully accredited by the Association for Assessment and Accreditation of Laboratory Animal Care and veterinary care was provided by Oregon Health & Science University's Department of Comparative Medicine. All animal care and experiments were performed in accordance with state and federal guidelines, and all protocols were approved by the OHSU Institutional Animal Care and Use Committee (protocol number: IP00001622). The authors understand the ethical principles of *The Journal of Physiology* and verify that the work in this manuscript complies with the journal's ethics checklist.

Slice Preparation and Electrophysiology:

Male and female mice were used between the ages of p21–30. KO and WT littermates were deeply anesthetized by inhalation of 4% isoflurane followed by injection of 0.8 ml of 2% avertin i.p. (Sigma-Aldrich, #T48402). Mice were then transcardially perfused with ice-cold choline-based solution containing (mM): 125 choline-Cl, 2.5 KCl, 1.25 NaH_2PO_4,

0.44 ascorbate, 2 Na pyruvate, 3 3-myo-inositol, 10 D-glucose, 25 $NaHCO_3$, 7 $MgCl_2$, 0.5 $CaCl_2$ (osmolarity adjusted to 305 mOsm) and equilibrated with 95% O_2 and 5% CO_2 gas mixture. Acute 300 μm sagittal slices were cut from cerebellum using a vibratome (VT1200, Leica Microsystems), and incubated for 30 minutes in standard artificial cerebral spinal fluid (aCSF) at 34°C.

Voltage clamp recordings:

Whole-cell recordings were obtained using 1–3 MΩ borosilicate glass pipettes filled with internal solution containing (in mM): 100 $CsMeSO_4$, 35 CsCl, 15 TEA-Cl, 1 $MgCl_2$, 15 HEPES, 2 ATP-Mg, 0.3 TrisGTP, 10 phosphocreatine, and 2 QX-314. A large batch of this internal base solution was equally divided and 10, 2 or 0.2 mM EGTA was added to each third. All internals were adjusted to pH 7.3 with CsOH and osmolarity to 293 mOsm. External solution contained (in mM): 125 NaCl, 25 $NaHCO_3$, 1.25 NaH_2PO_4, 3 KCl, 25 Dextrose, 2 $CaCl_2$, 1 $MgCl_2$ (osmolarity adjusted to 300 mOsm) and was continuously perfused via roller pump.

PCs were identified and recorded as previously described (Beeson et al., 2020). Briefly, PCs were chosen from the vermis lobe VI, were identified by soma size and location in the PC layer, and whole-cell patch-clamp recordings were obtained in voltage clamp mode. Cell capacitance, series resistance and input resistance monitored in real time using intermittent −10 mV voltage steps. Inhibition was blocked in all experiments by 10 μM SR95531 (Abcam, #ab120042), and 0.2–0.5 μM NBQX (Abcam, #ab120046) was included to maintain voltage clamp of climbing fiber-mediated excitatory postsynaptic currents (EPSCs). All voltage clamp recordings were performed at room temperature, as the magnitude of DSE is temperature-independent (Kreitzer & Regehr, 2001b). Signals were amplified with a MultiClamp 700B (Molecular Devices) amplifier and pipette capacitance was compensated using MultiClamp software. Signals were low-pass filtered at 6 kHz and sampled at 10 kHz, and digitized with a National Instruments analog-to-digital board. All recordings were acquired and analyzed using IgorPro-based (Wavemetrics) software.

Though physiological DSE (*in vivo*) likely is mediated by action-potential firing, brief depolarizing steps are widely used to reliably induce eCB release and DSE in acute slice preparations (Kreitzer & Regehr, 2001a, b; Maejima et al., 2001; Ohno-Shosaku et al., 2001; Wilson et al., 2001; Brown et al., 2004; Yoshino et al., 2011). For DSE experiments, PCs were held at −70 mV while climbing fiber-mediated EPSCs were evoked using a monopolar glass electrode in the granule cell layer. After obtaining 2 minutes of baseline responses at 0.2 Hz, a depolarizing voltage step to 0 mV of 1 s, 500 ms or 250 ms duration was delivered to induce DSE, after which PCs were returned to −70 mV and 0.2 Hz stimulation was continued. DSE plasticity is acute, and most synapses recover back to baseline EPSC amplitudes within < 60 seconds (Brenowitz & Regehr, 2003). As a small amount of “run down” was routinely observed in the evoked CF-mediated EPSC amplitude, DSE inclusion criteria required EPSC amplitudes to return to 80% baseline within 2 minutes post-stimulation (opposed to “stepping” to decreased amplitude without recovery). A minimum of 5 minutes were elapsed between DSE inductions, and step length was randomized throughout the experiments. For CB1R activation experiments, climbing fibers

were stimulated at 0.2 Hz while PCs were held at −70 mV and perfused with control aCSF (including 0.5 μM NBQX, 10 μM SR95531) plus DMSO or 5 μM WIN55,212–2 (Tocris, #1038). The effects of WIN55,212–2 wash-on were made by comparing the average EPSC amplitude from 1 minute of baseline recordings prior to WIN55,212–2 application, and the 1 minute average EPSC amplitude from after 15 minutes of wash-on. Series resistance was not compensated; cells with series resistance >10 MΩ, or with a >2 MΩ change in series resistance over the course of the experiment were excluded.

For analysis, EPSC amplitudes were binned every 10 seconds (2 traces) and normalized to the 1 minute of baseline immediately preceding the depolarizing step. The 'DSE magnitude' (e.g. Figure 1F) is based on the average of EPSC amplitude 5 and 10 s after the depolarizing step. Example traces shown are from 5 s after the depolarizing step. A minimum of 3 mice per genotype were used for each manipulation, with no more than 2 cells/treatment coming from one mouse. For data presentation, EPSC traces were off-line box-filtered at 1 kHz in Igor64 software.

Current clamp recordings:

For spontaneous spike experiments, internal solution contained (in mM): 120 KCH_3SO_3, 10 HEPES, 10 NaCl, 2 $MgCl_2$, 0.5 EGTA, 4 ATP-Mg, 0.3 Tris-GTP, and 14 phosphocreatine, pH 7.35 adjusted with KOH (osmolarity adjusted to 293 mOsm). A stock of EGTA solution was added to aliquots of internal, to increase [EGTA] to 5mM as needed, as this concentration is predicted to uncouple VGCCs from BK channels at a distance of >40 nm (Fakler & Adelman, 2008), the average distance between VGCCs and BK in Purkinje neurons (Indriati et al., 2013). Synaptic inhibition was achieved with 10 μM SR95531 and 10 μM NBQX, and recordings were made at 36°C using an in-line heater. PCs in whole-cell mode from vermis lobe VI were first held in voltage clamp mode to monitor access series and input resistance before switching to current clamp. Changes in access were corrected with bridge balance using Multiclamp software. For increased action potential waveform resolution, some current clamp experiments were sampled at 50 kHz.

Spontaneous spikes from tonically firing PCs with < 400 pA holding current and < 10 MOhm series were analyzed using the Igor64 Neuromatic tools. Firing frequency data was collected from 10 seconds of recording, which yielded ~100–500 spikes. Action potential properties were assessed by averaging 50 consecutive spikes. Afterhyperpolarization (AHP) amplitude was measured as the difference between the threshold voltage (V_{thres} = depolarization rate >10 V/s) and the minimum voltage reached within 5 ms of spiking. All current clamp data was taken at least 3 minutes after break-in to allow time for internal solution to dialyze. Spike traces were box filtered for data visualization, and phase plane plots were made using Igor64.

Immunohistochemistry:

Immunohistochemistry was performed as described (Beeson et al., 2020). Briefly, p21 WT and KO mice were deeply anesthetized as described above, and transcardially perfused with ice-cold PBS followed by 4% paraformaldehyde (PFA)-PBS. Following decapitation, brains were removed and fixed overnight in 4% PFA-PBS, and stored in PBS at 4°C. Sagittal

cerebellar slices were made at 50 μm thickness using a vibratome, and slices containing vermis lobe VI were permeabilized for 1 hr with 0.4% Triton-PBS with 10% normal horse serum at RT. Slices were stained with mouse anti-Calbindin (Antibodies Incorporated, #75–448; 1:20; (Holderith et al., 2020)), guinea pig anti-VGLUT2 (Synaptic Systems, #135–404; 1:200; (Purrier et al., 2014)), and rabbit anti-DGLa (Frontier Institute, #2571691; 1:400; (Uchigashima et al., 2011)), or goat anti-Parvalbumin (Swant, #PVG-213; 1:1000; (Schwaller et al., 1999)) and mouse anti-BK (Neuromab, #73–022; 1:500; (Martinez-Espinosa et al., 2014)) overnight at 4°C. Corresponding fluorescently labeled secondaries (Invitrogen; 1:500) were applied after rinsing 3x in PBS, and slices were mounted on glass cover slips using Fluoromount G (Sigma-Aldrich, #F4680).

BK/PV and DGLα/VGLUT2/Calbindin membrane expression was imaged using 63×1.4 NA oil immersion lens on a LSM980 microscope with ZEN software. For BK/PV, ~7 μm z-stack images of primary PC dendrites were acquired at 0.15 μm intervals using the PV channel at 4.5 × zoom with 680 × 680 pixel resolution; for DGLα/VGLUT2/Calbindin, 2.5 μm z-stack images of primary PC dendrites were acquired at 0.15 μm intervals using the Calbindin channel with 1840 × 1840 pixel resolution. Airyscan images were processed using default settings in ZEN. Quantification of membrane localized BK puncta or DGLα/VGLUT2 was done by a separate researcher, blinded to genotype. For BK quantification, the most transverse section of dendrite from each z-stack was analyzed and 0.45 μm maximum projections were used for the illustration in the figure. For DGLα/VGLUT2, a compilation of 5 consecutive images (0.75 μm stack) were cropped to illustrate a 25 × 25 μm region of interest. For presentation, images were processed in Fiji/ImageJ and the panel was assembled using Adobe Illustrator.

Statistics:

The data were tested for normality using Shapiro-Wilk test. Data from male and female mice were grouped as no sex differences were noted. For DSE, preliminary data was used to determine n with a power analysis designed to detect a difference of 50% between genotypes (with an assumed standard deviation of 25%) at a power of 80% and level of significance set to $p = 0.05$. The difference in magnitude of DSE between the WT 250 ms depolarization step condition (WT_{250}) and other groups were compared using a two-way ANOVA with Sidak's correction for multiple comparisons. For current clamp data, student's unpaired t-tests were used for spike frequency comparison between WT and KO. In current clamp experiments using 5 mM EGTA, only AHP amplitude was significantly different (all other measures not shown). For this data, a two-way ANOVA with Sidak's correction for multiple comparisons was used to compare all groups to WT 0.5 mM condition ($WT_{0.5}$). n = cells, each cell from a new slice, and each experiment from > 3 mice for all electrophysiology experiments with no more than 3 cells from one any animal per experiment. For immunohistochemistry of BK membrane density measurements, data from 2–4 images per animal were averaged (n = mice), and an unpaired t-test was used for comparison. Data were graphed in Prism GraphPad version 9.0.1 and are reported as the mean ± SD; *$p<0.05$, **$p<0.01$, ***$p<0.001$, **** $p < 0.0001$. All data for the conclusions of this study are reported in the manuscript.

Results

At PC climbing fiber synapses, postsynaptic voltage-dependent Ca^{2+} entry initiates retrograde endocannabinoid signaling, acutely reducing presynaptic release probability - a form of plasticity known as DSE (Brenowitz & Regehr, 2003; Brenowitz et al., 2006). It is presumed that postsynaptic VGCCs tightly couple with Ca^{2+}-sensitive endocannabinoid effector molecules, as high concentrations of fast Ca^{2+} buffers are required to block climbing fiber DSE (Kreitzer & Regehr, 2001b; Ohno-Shosaku et al., 2001; Brenowitz et al., 2006). Using whole-cell recordings of PCs in acutely prepared brain slices from *CACNA2D2* KO and WT littermate mice, we investigated whether absence of α2δ−2 affects DSE.

In WT PCs, DSE elicited with a 250 ms depolarizing step reduced the amplitude of regularly evoked climbing fiber excitatory postsynaptic currents (EPSCs) by 24.9 ± 18.5% (n = 6 cells from 3 mice; Fig 1A–D). In contrast, DSE was absent in KO PCs (3.6 ± 2.8%; n = 4 cells from 3 mice, p = 0.0283; Fig 1B–D). The *ducky* mouse, which also lacks α2δ−2 protein, has a ~30% decrease in PC somatic VGCC current density, which is thought to represent decreased VGCC surface trafficking (Donato et al., 2006). As DSE magnitude is related to the amount of Ca^{2+} influx (Brenowitz & Regehr, 2003), it is possible that the reduced VGCC density prevented DSE. However, although increasing the depolarizing step length enhances Ca^{2+} influx and DSE in WT mice (Brenowitz & Regehr, 2003), a four-fold increase in step duration still failed to evoke DSE in α2δ−2 KO PCs (Fig 1D–F; DSE Magnitude: WT_{500ms} = 20.4 ± 9.4%, n = 9 cells (4 mice); p = 0.951; WT_{1s} = 32.4 ± 15.1%, n = 12 cells (8 mice); p = 0.657; KO_{500ms} = 3.4 ± 0.9%, n = 5 cells (5 mice); p = 0.0156; KO_{1s} = 5.4 ± 4.4%, n = 10 cells (9 mice); p = 0.00930; Two-way ANOVA compared to WT_{250ms}, Sidak's correction for multiple comparisons).

This lack of DSE could not be explained by a failure of the presynaptic response to endocannabinoids, as activation of climbing fiber cannabinoid receptors (CB1Rs) by WIN55,212–2 (5 μM) equally reduced EPSC amplitudes in WT and KO Purkinje cells (% decrease in EPSC amplitude after 15 minutes of 5 μM WIN55,212–2: WT = 29.59 ± 15.24, n = 9; KO = 34.47 ± 6.578, n = 7; p = 0.445; Student's unpaired t-test; data are reported as mean ± SD), indicating that CB1R signaling is intact in both genotypes. Furthermore, we assessed the presence of a predominant eCB producing enzyme, diacylglycerol lipase α (DGLα), in WT and KO PCs by immunolabeling and confocal imaging. In all mice (n = 4/genotype), DAGα was visible at PC membranes and was localized within < 1μm of presynaptic climbing fiber terminals, which are identified by their VGLUT2+ immunohistochemistry (Fig 2). While eCB signaling remains highly complex, two critical components required for DSE, presynaptic CB1R activation and postsynaptic DGLα, appear normal in the α2δ−2 KO.

As DSE was not rescued by increased activation of VGCCs in KO PCs, we hypothesized that functional coupling of Ca^{2+} influx to effector molecules was disrupted in the absence of α2δ−2. To examine this, we lowered [EGTA] in our internal solution. As expected and illustrated in Table 1, decreasing [EGTA] from 10 mM to either 2 mM or 0.2 mM resulted in more profound DSE magnitude in WT PCs, which further increased with longer voltage

steps (Fig 3A–C), consistent with greater diffusion of Ca^{2+} from its point of entry. Notably, reduced Ca^{2+} buffering restored DSE in KO PCs (Fig 3D–F), demonstrating that when Ca^{2+} is allowed to diffuse further from its entry source, the downstream signaling mechanisms involved in DSE expression remained intact in KO mice. Thus, these data indicate that rather than affecting Ca^{2+} entry per se, α2δ−2 mediates tight functional coupling between VGCCs and endocannabinoid release, typical of nanodomain-dependent signaling.

To investigate whether α2δ−2 affects coupling of other effector molecules to postsynaptic VGCC nanodomains, we focused on Ca^{2+}-dependent afterhyperpolarizations (AHPs) following action potentials. In PCs, the AHP is mediated by BK-type K_{Ca} channels (Edgerton & Reinhart, 2003; Niday & Bean, 2021), and regulates PC firing rate (Raman & Bean, 1999; Womack et al., 2004). To assess VGCC-K_{Ca} coupling, which occurs at nanodomains throughout PC dendrites and soma (Indriati et al., 2013), we recorded spontaneous spiking in PCs from WT and KO mice during whole-cell current-clamp recordings. In agreement with previous studies in *ducky* mutants (Donato et al., 2006; Walter et al., 2006), tonic spike rate in α2δ−2 KO PCs (12.9 ± 11.4 Hz, n = 11 cells from 8 mice) was reduced compared to WT (Fig 4A–B; WT = 36.5 ± 15.8 Hz, n = 12 cells (10 mice); p = 0.0006; Student's unpaired t-test). Furthermore, AHP amplitude of individual spike waveforms was consistently smaller in α2δ−2 KO cells (Fig 4C–D; WT = 12.8 ± 3.18 mV, n = 12 cells (10 mice); KO = 8.18 ± 2.45 mV, n = 11 cells (8 mice); p < 0.0001), indicating reduced K_{Ca} channel activation (Edgerton & Reinhart, 2003; Womack et al., 2004). As shown in Table 2, other membrane properties were unchanged in KO PCs, including the resting membrane potential, membrane polarization rate, spike threshold and spike height (Fig 4E–J), indicating that changes in the KO were limited to the K_{Ca}-mediated AHP. Additionally, there was no change in the number of immunolabeled BK channel puncta in PCs (Fig 4K; Membrane BK density: WT = 0.819 ± 0.257 puncta/μm, n = 4 mice (2–4 images/mouse averaged); KO = 0.751 ± 0.134 puncta/μm, n = 3 mice (2–4 images/mouse averaged); p = 0.698; Student's unpaired t-test; data reported as the mean ± SD), consistent with normal BK expression and function, as previously described in *ducky* mice (Fell et al., 2016).

To determine whether the reduced AHP resulted from functionally uncoupled VGCC-K_{Ca} channels in KO mice, we dialyzed PCs with an increased EGTA concentration (from 0.5 mM to 5 mM) that uncouples VGCC-BK signaling (Fakler & Adelman, 2008). This additional Ca^{2+} buffering reduced the AHP amplitude in WT PCs to 9.93 ± 2.83 mV (n = 8 cells from 6 mice; p < 0.0001) to the same value as the KO AHP. In contrast, the KO AHP did not change with increased EGTA (Fig 4C–D; KO_5 = 8.98 ± 3.44 mV, n = 8 cells (5 mice); p < 0.0001; Two-way ANOVA comparison to WT 0.5 mM EGTA response ($WT_{0.5}$) with Sidak's correction for multiple comparisons; data reported as the mean ± SD). Thus, increased Ca^{2+} buffering uncoupled VGCC-K_{Ca} signaling in WT, but K_{Ca} channels were already uncoupled in the α2δ−2 KO.

Discussion

As a primary signal in neurons, precise spatiotemporal regulation of Ca^{2+} influx maintains fidelity of Ca^{2+}-dependent processes in neurons. Consequently, molecules controlling

VGCC coupling to downstream effectors are critical to neuronal function. α2δ proteins are involved in trafficking of VGCCs to the plasma membrane (Dolphin & Lee, 2020) – a conclusion largely based on observations made in heterologous expression systems. However, most neurons express more than one α2δ isoform, making loss-of-function analyses more challenging. For this reason, appreciation of other postsynaptic auxiliary functional roles of α2δ proteins in neurons is limited. Because PCs selectively express the α2δ−2 isoform (Lein et al., 2007; Beeson et al., 2020), the *CACNA2D2* KO mouse provides an ideal model in which to examine the functional roles for α2δ proteins in the postsynaptic compartment. Our results demonstrate that two distinct postsynaptic Ca^{2+}-dependent mechanisms, DSE and K_{Ca} signaling, are disrupted in α2δ−2 KO PCs, indicating functional loss of voltage-dependent calcium coupling. Though upregulation of other α2δ isoforms could potentially compensate for α2δ−2 loss in the KO, the robust functional phenotypes found here indicate that this does not occur, and when directly examined, we and others (Schopf et al., 2021) have not detected changes in other α2δ isoform mRNA levels after deletion of α2δ−2.

Given the challenges of visualizing endogenous VGCCs or α2δ proteins in tissues, and the complexity of calcium-dependent eCB synthesis and signaling, it is unclear which molecules are specifically mislocalized in the absence of α2δ−2 proteins. Although the source of Ca^{2+} involved in DSE-induction has not been defined in Purkinje cells, our voltage-step protocol likely activated VGCCs on the plasma membrane as well as release from intracellular stores, producing a graded influx of Ca^{2+} dependent on duration of depolarization (Brenowitz & Regehr, 2003). Regardless, the voltage-activated Ca^{2+} signal is normally tightly-coupled to eCB-producing effector molecules, as evidenced by the high concentrations of fast Ca^{2+} buffers required to block eCB signaling (Kreitzer & Regehr, 2001a; Ohno-Shosaku et al., 2001; Brenowitz et al., 2006). Because NMDARs are not present at the mouse climbing fiber synapse until late adulthood (Piochon et al., 2007; Renzi et al., 2007; but also see Rosenmund et al., 1992), and our DSE induction protocol did not pair glutamate release with postsynaptic depolarization, it is unlikely that NMDARs, for example, would serve as an alternative source of Ca^{2+}.

Presynaptic CFs in α2δ−2 KO mice demonstrate a reduced probability of release, but overall enhanced glutamate release due to increased CF synapse formation (Beeson et al., 2020), suggesting possible changes in presynaptic VGCC signaling in the KO. However, our findings that presynaptic activation of CB1-type cannabinoid receptors by application of WIN55,212–2 produced an equivalent suppression of evoked release to that of WT CFs, and that changes in postsynaptic Ca^{2+} buffering revealed DSE in the KO, indicate that all requirements for eCB-mediated plasticity are present and functional despite the loss of α2δ−2 proteins. Nonetheless, the effect of postsynaptic EGTA manipulations on eCB-mediated signaling in the KO suggests a change in the effectiveness of postsynaptic voltage-dependent Ca^{2+} signaling to eCB effectors, possibly via VGCCs on the plasma membrane. Careful identification of the exact DSE signaling effectors involved in α2δ-mediated coupling, and the specific protein-protein interactions mediating their proximal localization, should be the focus of future studies.

How might α2δ−2, a largely extracellular protein, mediate functional coupling of VGCCs with intracellular effector proteins like those involved in eCB signaling? It is possible that α2δ−2 directly associates with other extracellular proteins involved in VGCC domains (Dolphin & Lee, 2020). As endocannabinoid machinery resides at synapses (Rimmerman et al., 2008), and α2δ proteins are important for synapse formation (Cole et al., 2005; Lein et al., 2007; Eroglu et al., 2009; Beeson et al., 2020), α2δ could participate in assembling functional VGCC nanodomains by binding to presynaptic adhesion proteins, thus localizing VGCCs at synapses. Another possibility is that α2δ−2 localizes VGCCs to lipid rafts. Though VGCCs are abundant in non-lipid raft membrane fractions where they are independent of α2δ−2, VGCCs and α2δ−2 colocalize in lipid rafts isolated from cerebellar homogenates (Davies et al., 2006). Intriguingly, DGLα has also been isolated in lipid rafts (Rimmerman et al., 2008), and mislocalization of VGCCs away from lipid rafts might explain the reduced efficacy of VGCC-signaling in α2δ−2 KO PCs. In regards to VGCC-K_{Ca} coupling, the α2δ−1 isoform interacts directly with BK channels in heterologous systems (Zhang et al., 2018), raising the possibility that this interaction occurs with other α2δ isoforms, including α2δ−2 in neurons.

Our results provide clues for future work to directly assay how α2δ−2 proteins contribute to Ca^{2+}-effector coupling in both K_{Ca} and eCB signaling systems, as many questions remain answered. For example, does pharmacological interference with α2δ-proteins by the potent and widely-used α2δ−1/2 therapeutic, gabapentin, impact Ca^{2+} coupling? Similar to electrophysiological studies of hippocampal neuron transmission (Brown & Randall, 2005), we found no effect of acute application of gabapentin on climbing fiber DSE in preliminary studies. However, chronic exposure to gabapentin may produce changes in α2δ-mediated Ca^{2+} coupling, as prolonged incubation (days) reduces α2δ−1-induced synapse formation and α2δ−1 recycling (Eroglu et al., 2009; Tran-Van-Minh & Dolphin, 2010). Gabapentin's mechanism(s) of action remain unclear, rendering our negative result of its impact on climbing fiber DSE inconclusive. Future research should also reveal whether α2δ isoforms perform differing functions in the neuron, or whether gabapentin exerts dissimilar effects on α2δ−1 vs. α2δ−2. Likewise, the potential involvement of other α2δ isoforms in neuronal VGCC nanodomain signaling may provide insights into how this family of proteins impact neurological functions across the brain.

Supplementary Material

Refer to Web version on PubMed Central for supplementary material.

Acknowledgments:

This research was supported by VA I01-BX002949 (ES) and I01-BX004938 (ES), DoD W81XWH-18-1-0598 (ES), NIH T32NS007466 (KAB), NIH P30NS061800 (OHSU), and NINDS 1R21NS102948 (Ines Koerner/ES). The contents of this manuscript do not represent the views of the U.S. Department of Veterans Affairs or the United States Government.

First Author Profile

Kathleen Beeson received her B.A. in Neuroscience from Knox College (2009) with an interest in synaptic physiology, and gained research experience as a technician studying adhesion molecules. She joined the Neuroscience Graduate Program at Oregon Health and Science University (2014), where she studied the synaptogenic and calcium signaling roles of α2δ proteins in neurons in the lab of Dr. Eric Schnell. She earned her PhD in 2021, and will continue to study how molecular interactions and organization inform synaptic function during her postdoctoral training at Harvard Medical School.

References

Beeson KA, Beeson R, Westbrook GL & Schnell E. (2020). alpha2delta-2 Protein Controls Structure and Function at the Cerebellar Climbing Fiber Synapse. J Neurosci 40, 2403–2415. [PubMed: 32086258]

Brenowitz SD, Best AR & Regehr WG. (2006). Sustained elevation of dendritic calcium evokes widespread endocannabinoid release and suppression of synapses onto cerebellar Purkinje cells. J Neurosci 26, 6841–6850. [PubMed: 16793891]

Brenowitz SD & Regehr WG. (2003). Calcium dependence of retrograde inhibition by endocannabinoids at synapses onto Purkinje cells. The Journal of Neuroscience 23, 6373–6384. [PubMed: 12867523]

Brown J & Randall A. (2005). Gabapentin Fails to Alter P/Q-type Ca2+ Channel-Mediated Synaptic Transmission in the Hippocampus In Vitro. Synapse 55, 262–269. [PubMed: 15668986]

Brown SP, Safo PK & Regehr WG. (2004). Endocannabinoids inhibit transmission at granule cell to Purkinje cell synapses by modulating three types of presynaptic calcium channels. J Neurosci 24, 5623–5631. [PubMed: 15201335]

Cole RL, Lechner SM, Williams ME, Prodanovich P, Bleicher L, Varney MA & Gu G. (2005). Differential distribution of voltage-gated calcium channel alpha-2 delta (alpha2delta) subunit mRNA-containing cells in the rat central nervous system and the dorsal root ganglia. J Comp Neurol 491, 246–269. [PubMed: 16134135]

Davies A, Douglas L, Hendrich J, Wratten J, Tran Van Minh A, Foucault I, Koch D, Pratt WS, Saibil HR & Dolphin AC. (2006). The calcium channel alpha2delta-2 subunit partitions with CaV2.1 into lipid rafts in cerebellum: implications for localization and function. J Neurosci 26, 8748–8757. [PubMed: 16928863]

Dolphin AC & Lee A. (2020). Presynaptic calcium channels: specialized control of synaptic neurotransmitter release. Nat Rev Neurosci 21, 213–229. [PubMed: 32161339]

Donato R, Page KM, Koch D, Nieto-Rostro M, Foucault I, Davies A, Wilkinson T, Rees M, Edwards FA & Dolphin AC. (2006). The ducky(2J) mutation in Cacna2d2 results in reduced spontaneous Purkinje cell activity and altered gene expression. J Neurosci 26, 12576–12586. [PubMed: 17135419]

Edgerton JR & Reinhart PH. (2003). Distinct contributions of small and large conductance Ca2+-activated K+ channels to rat Purkinje neuron function. J Physiol 548, 53–69. [PubMed: 12576503]

Eroglu C, Allen NJ, Susman MW, O'Rourke NA, Park CY, Ozkan E, Chakraborty C, Mulinyawe SB, Annis DS, Huberman AD, Green EM, Lawler J, Dolmetsch R, Garcia KC, Smith SJ, Luo ZD, Rosenthal A, Mosher DF & Barres BA. (2009). Gabapentin receptor alpha2delta-1 is a neuronal thrombospondin receptor responsible for excitatory CNS synaptogenesis. Cell 139, 380–392. [PubMed: 19818485]

Fakler B & Adelman JP. (2008). Control of K(Ca) channels by calcium nano/microdomains. Neuron 59, 873–881. [PubMed: 18817728]

Fell B, Eckrich S, Blum K, Eckrich T, Hecker D, Obermair GJ, Munkner S, Flockerzi V, Schick B & Engel J. (2016). alpha2delta2 Controls the Function and Trans-Synaptic Coupling of Cav1.3 Channels in Mouse Inner Hair Cells and Is Essential for Normal Hearing. J Neurosci 36, 11024–11036. [PubMed: 27798183]

Holderith N, Heredi J, Kis V & Nusser Z. (2020). A High-Resolution Method for Quantitative Molecular Analysis of Functionally Characterized Individual Synapses. Cell Rep 32, 107968. [PubMed: 32726631]

Hoppa MB, Lana B, Margas W, Dolphin AC & Ryan TA. (2012). alpha2delta expression sets presynaptic calcium channel abundance and release probability. Nature 486, 122–125. [PubMed: 22678293]

Indriati DW, Kamasawa N, Matsui K, Meredith AL, Watanabe M & Shigemoto R. (2013). Quantitative localization of Cav2.1 (P/Q-type) voltage-dependent calcium channels in Purkinje cells: somatodendritic gradient and distinct somatic coclustering with calcium-activated potassium channels. J Neurosci 33, 3668–3678. [PubMed: 23426693]

Kreitzer AC & Regehr WG. (2001a). Cerebellar Depolarization-Induced Suppression of Inhibition Is Mediated by Endogenous Cannabinoids. The Journal of Neuroscience 21.

Kreitzer AC & Regehr WG. (2001b). Retrograde Inhibition of Presynaptic Calcium Influx by Endogenous Cannabinoids at Excitatory Synapses onto Purkinje Cells. Neuron 29, 10.

Kurshan PT, Oztan A & Schwarz TL. (2009). Presynaptic alpha2delta-3 is required for synaptic morphogenesis independent of its Ca2+-channel functions. Nat Neurosci 12, 1415–1423. [PubMed: 19820706]

Lein ES, Hawrylycz MJ, Ao N, Ayres M, Bensinger A, Bernard A, Boe AF, Boguski MS, Brockway KS, Byrnes EJ, Chen L, Chen L, Chen TM, Chin MC, Chong J, Crook BE, Czaplinska A, Dang CN, Datta S, Dee NR, Desaki AL, Desta T, Diep E, Dolbeare TA, Donelan MJ, Dong HW, Dougherty JG, Duncan BJ, Ebbert AJ, Eichele G, Estin LK, Faber C, Facer BA, Fields R, Fischer SR, Fliss TP, Frensley C, Gates SN, Glattfelder KJ, Halverson KR, Hart MR, Hohmann JG, Howell MP, Jeung DP, Johnson RA, Karr PT, Kawal R, Kidney JM, Knapik RH, Kuan CL, Lake JH, Laramee AR, Larsen KD, Lau C, Lemon TA, Liang AJ, Liu Y, Luong LT, Michaels J, Morgan JJ, Morgan RJ, Mortrud MT, Mosqueda NF, Ng LL, Ng R, Orta GJ, Overly CC, Pak TH, Parry SE, Pathak SD, Pearson OC, Puchalski RB, Riley ZL, Rockett HR, Rowland SA, Royall JJ, Ruiz MJ, Sarno NR, Schaffnit K, Shapovalova NV, Sivisay T, Slaughterbeck CR, Smith SC, Smith KA, Smith BI, Sodt AJ, Stewart NN, Stumpf KR, Sunkin SM, Sutram M, Tam A, Teemer CD, Thaller C, Thompson CL, Varnam LR, Visel A, Whitlock RM, Wohnoutka PE, Wolkey CK, Wong VY, Wood M, Yaylaoglu MB, Young RC, Youngstrom BL, Yuan XF, Zhang B, Zwingman TA & Jones AR. (2007). Genome-wide atlas of gene expression in the adult mouse brain. Nature 445, 168–176. [PubMed: 17151600]

Maejima T, Ohno-Shosaku T & Kano M. (2001). Endogenous cannabinoid as a retrograde messenger from depolarized postsynaptic neurons to presynaptic terminals. Neurosci Res 40, 205–210. [PubMed: 11448511]

Martinez-Espinosa PL, Yang C, Gonzalez-Perez V, Xia XM & Lingle CJ. (2014). Knockout of the BK beta2 subunit abolishes inactivation of BK currents in mouse adrenal chromaffin cells and results in slow-wave burst activity. J Gen Physiol 144, 275–295. [PubMed: 25267913]

Niday Z & Bean BP. (2021). BK Channel Regulation of Afterpotentials and Burst Firing in Cerebellar Purkinje Neurons. J Neurosci 41, 2854–2869. [PubMed: 33593855]

Ohno-Shosaku T, Maejima T & Kano M. (2001). Endogenous cannabinoids mediate retrograde signals from depolarized postsynaptic neurons to presynaptic terminals. Neuron 29, 729–738. [PubMed: 11301031]

Piochon C, Irinopoulou T, Brusciano D, Bailly Y, Mariani J & Levenes C. (2007). NMDA receptor contribution to the climbing fiber response in the adult mouse Purkinje cell. J Neurosci 27, 10797–10809. [PubMed: 17913913]

Purrier N, Engeland WC & Kofuji P. (2014). Mice deficient of glutamatergic signaling from intrinsically photosensitive retinal ganglion cells exhibit abnormal circadian photoentrainment. PLoS One 9, e111449. [PubMed: 25357191]

Raman IM & Bean BP. (1999). Ionic Currents Underlying Spontaneous Action Potentials in Isolated Cerebellar Purkinje Neurons. Journal of Neuroscience 19, 12.

Renzi M, Farrant M & Cull-Candy SG. (2007). Climbing-fibre activation of NMDA receptors in Purkinje cells of adult mice. J Physiol 585, 91–101. [PubMed: 17901118]

Rimmerman N, Hughes HV, Bradshaw HB, Pazos MX, Mackie K, Prieto AL & Walker JM. (2008). Compartmentalization of endocannabinoids into lipid rafts in a dorsal root ganglion cell line. Br J Pharmacol 153, 380–389. [PubMed: 17965731]

Rosenmund C, Legendre P & Westbrook GL. (1992). Expression of NMDA channels on cerebellar Purkinje cells acutely dissociated from newborn rats. J Neurophysiol 68, 1901–1905. [PubMed: 1282541]

Schopf CL, Ablinger C, Geisler SM, Stanika RI, Campiglio M, Kaufmann WA, Nimmervoll B, Schlick B, Brockhaus J, Missler M, Shigemoto R & Obermair GJ. (2021). Presynaptic alpha2delta subunits are key organizers of glutamatergic synapses. Proc Natl Acad Sci U S A 118.

Schwaller B, Bruckner G, Celio MR & Hartig W. (1999). A polyclonal goat antiserum against the calcium-binding protein calretinin is a versatile tool for various immunochemical techniques. J Neurosci Methods 92, 137–144. [PubMed: 10595711]

Tran-Van-Minh A & Dolphin AC. (2010). The alpha2delta ligand gabapentin inhibits the Rab11-dependent recycling of the calcium channel subunit alpha2delta-2. J Neurosci 30, 12856–12867. [PubMed: 20861389]

Uchigashima M, Yamazaki M, Yamasaki M, Tanimura A, Sakimura K, Kano M & Watanabe M. (2011). Molecular and morphological configuration for 2-arachidonoylglycerol-mediated retrograde signaling at mossy cell-granule cell synapses in the dentate gyrus. J Neurosci 31, 7700–7714. [PubMed: 21613483]

Walter JT, Alvina K, Womack MD, Chevez C & Khodakhah K. (2006). Decreases in the precision of Purkinje cell pacemaking cause cerebellar dysfunction and ataxia. Nat Neurosci 9, 389–397. [PubMed: 16474392]

Wilson RI, Kunos G & Nicoll RA. (2001). Presynaptic specificity of endocannabinoid signaling in the hippocampus. Neuron 31, 453–462. [PubMed: 11516401]

Womack MD, Chevez C & Khodakhah K. (2004). Calcium-activated potassium channels are selectively coupled to P/Q-type calcium channels in cerebellar Purkinje neurons. J Neurosci 24, 8818–8822. [PubMed: 15470147]

Yoshino H, Miyamae T, Hansen G, Zambrowicz B, Flynn M, Pedicord D, Blat Y, Westphal RS, Zaczek R, Lewis DA & Gonzalez-Burgos G. (2011). Postsynaptic diacylglycerol lipase mediates retrograde endocannabinoid suppression of inhibition in mouse prefrontal cortex. J Physiol 589, 4857–4884. [PubMed: 21807615]

Zhang FX, Gadotti VM, Souza IA, Chen L & Zamponi GW. (2018). BK Potassium Channels Suppress Cavalpha2delta Subunit Function to Reduce Inflammatory and Neuropathic Pain. Cell Rep 22, 1956–1964. [PubMed: 29466724]

Key Points Summary

- Calcium influx, via voltage-dependent calcium channels, drives numerous neuronal signaling processes with precision achieved in part by tight coupling between calcium entry and calcium-dependent effectors.
- α2δ proteins are important for neurological function and contribute to calcium channel membrane trafficking, although how α2δ proteins influence postsynaptic calcium-dependent signaling is largely unexplored.
- Here we report that loss of α2δ−2 proteins disrupts functional calcium coupling to two different postsynaptic calcium-dependent signals in mouse Purkinje cell neurons, retrograde endocannabinoid signaling and the action potential afterhyperpolarization.
- Our findings provide new insights about the control of calcium coupling as well as new roles for α2δ−2 proteins in neurons.

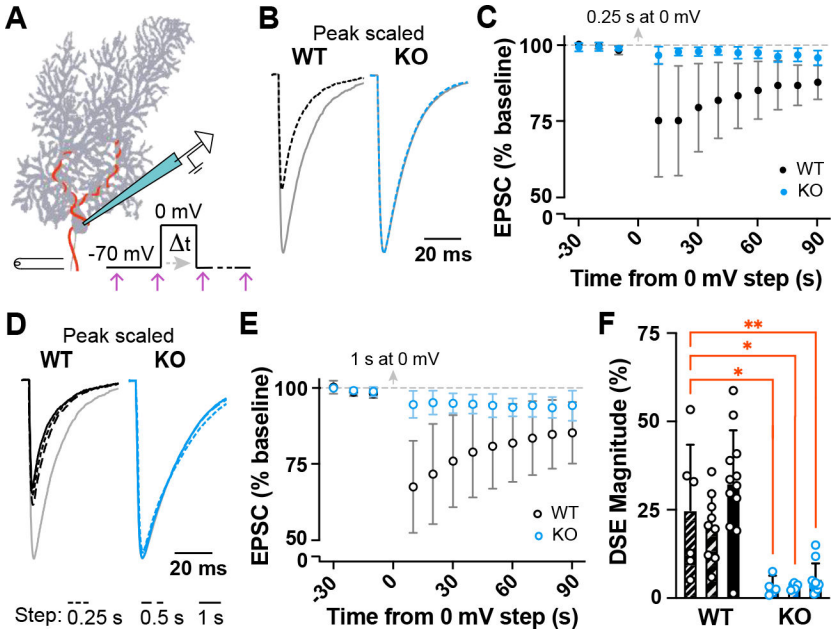

Figure 1. Depolarization-Induced Suppression of Excitation (DSE) reduces climbing fiber-EPSC amplitude in WT but not α2δ−2 KO Purkinje cells.

A) Experimental schematic. Purkinje cell (PC) is held at −70 mV while the climbing fiber axon (red) is stimulated at 0.2 Hz (arrows). A depolarization step to 0 mV is delivered to the PC between EPSC recordings.

B) Overlay of peak-scaled EPSC traces during baseline (grey) and 5 s post-depolarization (dotted line) from WT (black) and KO (blue) PCs; 250 ms step duration.

C) Summary of WT and KO timecourse responses to 250 ms depolarization shown as % of baseline EPSC. Each point averaged two consecutive EPSCs. WT (black, filled circle): 24.9 ± 18.5% (n = 6 cells from 3 mice; KO (blue, filled circle): 3.6 ± 2.8%; n = 4 cells from 3 mice; data are reported as the mean ± SD.

D) Overlay of peak-scaled EPSCs during baseline (grey) and 5 s after 250 ms (dotted line), 500 ms (dashed line), and 1 s (solid line) depolarization from WT (black) and KO (blue) PCs.

E) DSE timecourse from WT (black, open circle) and KO (blue, open circle) experiments using 1 s depolarizing step lengths shown as % of baseline EPSC. Each point averaged two consecutive EPSCs. WT_{1s} = 32.4 ± 15.1%, n = 12 cells (8 mice); KO_{1s} = 5.4 ± 4.4%, n = 10 cells (9 mice); data are reported as the mean ± SD.

F) EPSC depression normalized to baseline (Magnitude of DSE) in WT (black) and KO (blue) after 250 ms (fine stripe), 500 ms (wide stripe) and 1 s (solid) depolarization steps: WT_{250ms} = 24.9 ± 18.5%, n = 6 cells (3 mice); WT_{500ms} = 20.4 ± 9.4%, n = 9 cells (4 mice); p = 0.951; WT_{1s} = 32.4 ± 15.1%, n = 12 cells (8 mice); p = 0.657; KO_{250ms} = 3.6 ± 2.8%, n = 4 cells (3 mice); p = 0.0283; KO_{500ms} = 3.4 ± 0.9%, n = 5 cells (5 mice); p = 0.0156; KO_{1s} = 5.4 ± 4.4%, n = 10 cells (9 mice); p = 0.00930; Two-way ANOVA compared to WT_{250ms}, Sidak's correction for multiple comparisons; data are reported as the mean ± SD; * $p < 0.05$, ** $p < 0.01$.

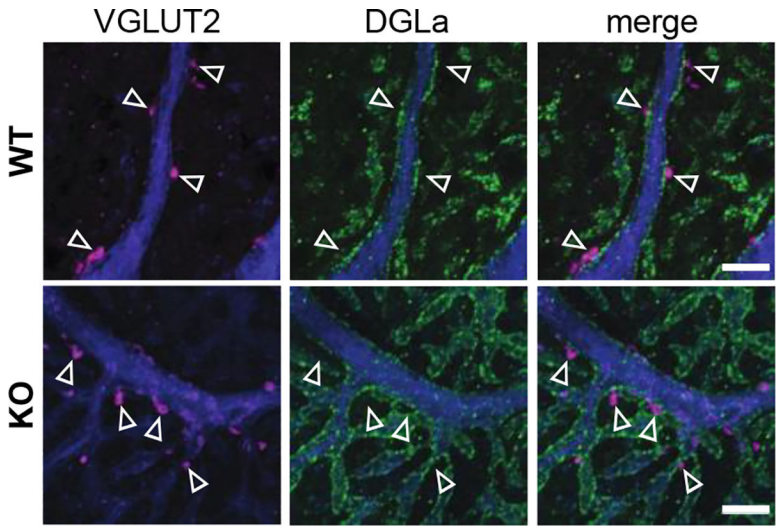

Figure 2. Endocannabinoid-producing enzymes are present near climbing fiber synapses in Purkinje cells of both genotypes.

Purkinje cells from WT (top) and KO (bottom) mice express the eCB-producing enzyme, diacylglycerol lipase α (DGLα; green), along dendritic membranes (calbindin; blue) adjacent to presynaptic climbing fiber synapses (VGLUT2; magenta), indicated by arrows. Scale bar 5 μm. Representative images shown are max projection confocal images, 63×1.4 NA objective.

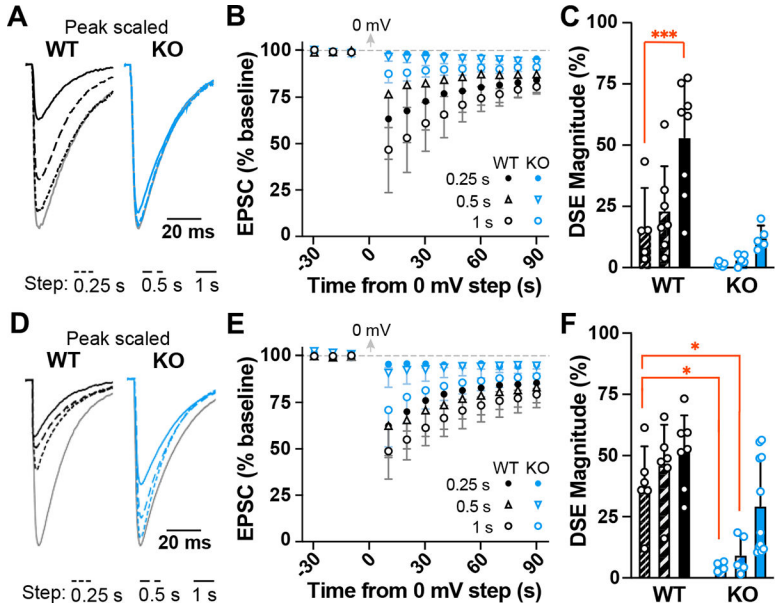

Figure 3. Reduced intracellular [EGTA] reveals DSE in the α2δ−2 KO.

A) Overlay of peak-scaled EPSCs during baseline (grey) and 5 s after 250 ms (dotted line), 500 ms (dashed line), and 1 s (solid line) depolarization using intracellular solution containing 2 mM EGTA from WT (black) and KO (blue) PCs.

B) DSE timecourse from WT (black) and KO (blue) experiments using 2 mM EGTA and depolarization steps of 250 ms (filled circle), 500 ms (triangle) and 1 s (open circle). Data are reported as the mean ± SD.

C) DSE Magnitude in WT (black) and KO (blue) after 250 ms (fine stripe), 500 ms (wide stripe) and 1 s (solid) depolarization steps using a 2 mM EGTA: WT_{250ms} = 16.8 ± 15.8%, 5 cells (4 mice); WT_{500ms} = 23.2 ± 18.1%, 7 cells (4 mice); p = 0.958; WT_{1s} = 53.2 ± 23.2%, n = 8 cells (5 mice); p = 0.000992; KO_{250ms} = 1.6 ± 0.8%, n = 6 cells (5 mice); p = 0.432; KO_{500ms} = 3.2 ± 2.2%, n = 5 cells (5 mice); p = 0.597; KO_{1s} = 12.2 ± 4.9%, n = 5 cells (5 mice); 0.994; Two-way ANOVA compared to WT_{250ms}, Sidak's correction for multiple comparisons; data are reported as the mean ± SD. *** p < 0.001.

D) Overlay of peak-scaled EPSCs during baseline (grey) and 5 s after 250 ms (dotted line), 500 ms (dashed line), and 1 s (solid line) depolarization using 0.2 mM EGTA from WT (black) and KO (blue) PCs.

E) DSE timecourse from WT (black) and KO (blue) experiments using 0.2 mM EGTA and depolarization steps of 250 ms (filled circle), 500 ms (triangle) and 1 s (open circle). Data are reported as the mean ± SD.

F) DSE Magnitude in WT (black) and KO (blue) after 250 ms (fine stripe), 500 ms (wide stripe) and 1 s (solid) depolarization steps using a 0.2 mM EGTA: WT_{250ms} = 38.0 ± 15.9%, n = 6 cells (4 mice); WT_{500ms} = 46.2 ± 16.5%, n = 6 cells (4 mice); p = 0.900; WT_{1s} = 51.6 ± 15.0%, n = 7 cells (4 mice); p = 0.493; KO_{250ms} = 4.8 ± 1.9%, n = 4 cells (3 mice); p = 0.0123; KO_{500ms} = 9.4 ± 7.8%, n = 5 cells (3 mice); p = 0.0250; KO_{1s} = 29.5 ± 19.7%, n = 11 cells (8 mice); p = 0.826; Two-way ANOVA compared to WT_{250ms}, Sidak's correction for multiple comparisons; data are reported as the mean ± SD. * p < 0.05.

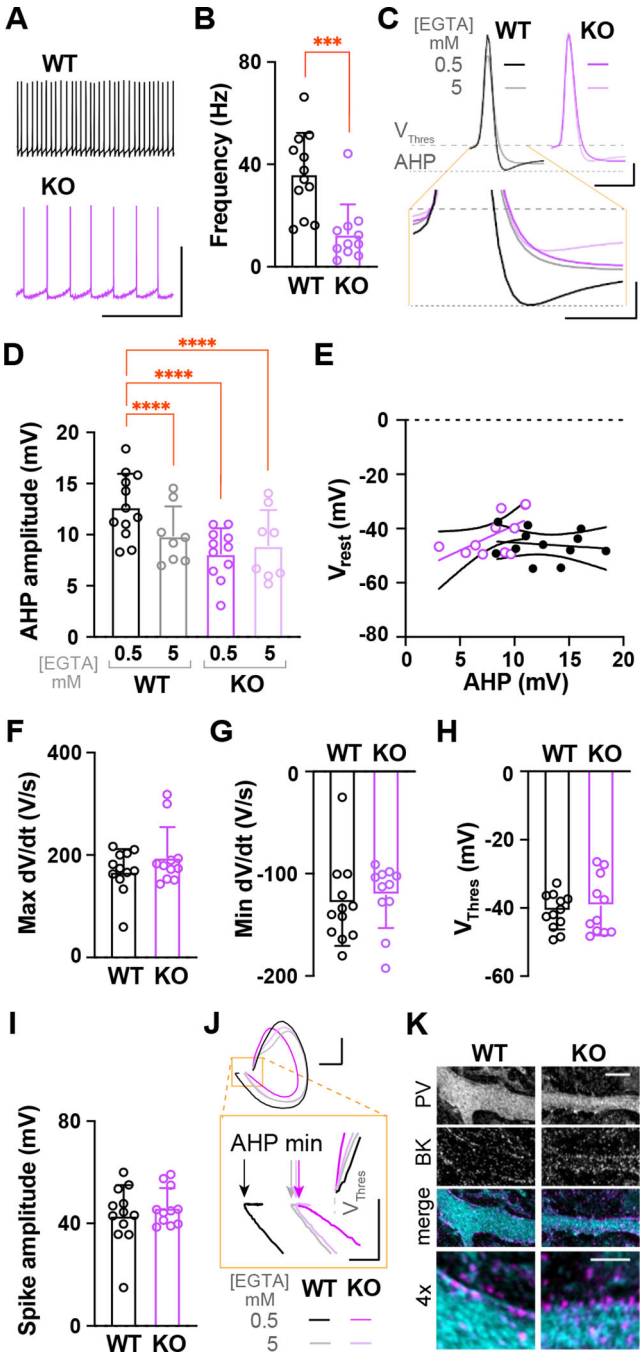

Figure 4. Spontaneous firing frequency, afterhyperpolarization (AHP) amplitude and Ca^{2+} coupling are reduced in the α2δ−2 KO.

A) Spontaneous spikes in WT (black) and KO (magenta) PCs; scale: 50 mV, 0.5 s.

B) Spontaneous firing frequency in PCs: WT = 36.5 ± 15.8 Hz, n = 12 cells (10 mice); KO = 12.9 ± 11.4 Hz, n = 11 cells (8 mice); p = 0.0006; Student's unpaired t-test; data are reported as the mean ± SD; *** p < 0.001.

C) Averaged spontaneous spikes from WT and KO PCs during tonic firing (0.5 mM EGTA, black/magenta; 5 mM EGTA grey/light purple); scale: 10 mV, 2 ms. Grey dotted lines

indicate V_{thres} and minimum voltage during AHP. *Below*, enlarged overlay demonstrating differences in AHP amplitude; scale: 5 mV, 1 ms.

D) AHP amplitudes recorded using 0.5 mM EGTA or 5 mM EGTA intracellular solution: $WT_{0.5}$ = 12.8 ± 3.18 mV, n = 12 cells (10 mice); WT_5 = 9.93 ± 2.83 mV, n = 8 cells (6 mice); p < 0.0001; $KO_{0.5}$ = 8.18 ± 2.45 mV, n = 11 cells (8 mice); p < 0.0001; KO_5 = 8.98 ± 3.44 mV, n = 8 cells (5 mice); p < 0.0001; Two-way ANOVA comparison to WT 0.5 mM EGTA response ($WT_{0.5}$) with Sidak's correction for multiple comparisons; data are reported as the mean + SD; **** p < 0.0001.

E) No correlation of AHP amplitude vs. resting membrane potential (V_m) in WT (black) and KO (magenta) PCs using 0.5 mM EGTA. Linear regression, slope mean and 95% confidence interval; WT R^2 = 0.00185; −0.0673, 95% CI [−1.17, 1.03]; KO R^2 = 0.393; 2.16, 95% CI [0.137, 4.19].

F-I) No differences in spike waveform parameters in WT and KO PCs. (**F**) Maximum dV/dt: $WT_{0.5}$ = 169 ± 42.6 dV/dt; $KO_{0.5}$ = 196 ± 58.2 dV/dt; p = 0.217; (**G**) Minimum dV/dt: $WT_{0.5}$ = −130 ± 40.9 dV/dt; $KO_{0.5}$ = −121 ± 31.7 dV/dt; p = 0.594; (**H**) Spike threshold (V_{thres}): $WT_{0.5}$ = −41.1 ± 5.19 mV; $KO_{0.5}$ = −39.5 ± 8.50 mV; p = 0.591; (**I**) Spike height: $WT_{0.5}$ = 43.4 ± 11.6 mV; $KO_{0.5}$ = 46.4 ± 7.42 mV; p = 0.462; unpaired Student's t-tests; data are reported as the mean ± SD; $WT_{0.5}$ n = 12 cells (10 mice); $KO_{0.5}$ n = 11 cells (8 mice).

J) Phase plane plots of spontaneous spikes in WT and KO PCs (0.5 mM EGTA, black/magenta; 5 mM EGTA grey/light purple). Traces aligned by spike threshold (V_{thresh}) for comparison; scale: 100 mV/ms, 20 mV. *Below*, enlarged inset to illustrate differences in AHP minimum amplitude (arrows; 0.5 mM EGTA, black/magenta; 5 mM EGTA, grey/light purple); scale: 100 mV/ms, 5 mV.

K) Immunohistochemistry of WT and KO cerebellar slices stained for parvalbumin (PV; cyan) and the BK channel (magenta); scale: 5 μm. *Below*, merged higher power image; scale: 2 μm. Images shown are max projection confocal images, 63×1.4 NA objective.

Author Manuscript

Author Manuscript

Author Manuscript

Table 1

	DSE magnitude using 2 mM EGTA internal			DSE magnitude using 0.2 mM EGTA internal		
	DSE Magnitude	**n**	**p value**	**DSE Magnitude**	**n**	**p value**
WT_{250ms}	16.8 ± 15.8%	5 cells (4 mice)		38.0 ± 15.9%	6 cells (4 mice)	
WT_{500ms}	23.2 ± 18.1%	7 cells (4 mice)	0.958	46.2 ± 16.5%	6 cells (4 mice)	0.900
WT_{1s}	53.2 ± 23.2%	8 cells (5 mice)	0.000992	51.6 ± 15.0%	7 cells (4 mice)	0.493
KO_{250ms}	1.6 ± 0.8%	6 cells (5 mice)	0.432	4.8 ± 1.9%	4 cells (3 mice)	0.0123
KO_{500ms}	3.2 ± 2.2%	5 cells (5 mice)	0.597	9.4 ± 7.8%	5 cells (3 mice)	0.0250
KO_{1s}	12.2 ± 4.9%	5 cells (5 mice)	0.994	29.5 ± 19.7%	11 cells (8 mice)	0.826

n = cells, each cell from a new slice, and each experiment from > 3 mice; Two-way ANOVA compared to WT_{250ms}, Sidak's correction for multiple comparisons; data are reported as the mean ± SD.

Author Manuscript

Author Manuscript

Author Manuscript

Table 2

Spontaneous spike membrane properties

	$WT_{0.5}$ Mean ± SD	**$KO_{0.5}$ Mean ± SD**	**p value**
Membrane potential (V_m)	−45.9 ± 5.60 mV	−42.2 ± 7.64 mV	0.190
Maximum dV/dt	169 ± 42.6 dV/dt	196 ± 58.2 dV/dt	0.217
Minimum dV/dt	−130 ± 40.9 dV/dt	−121 ± 31.7 dV/dt	0.594
Spike threshold (V_{thres})	−41.1 ± 5.19 mV	−39.5 ± 8.50 mV	0.591
Spike height	43.4 ± 11.6 mV	46.4 ± 7.42 mV	0.462

$WT_{0.5}$ n = 12 cells (10 mice); $KO_{0.5}$ n = 11 cells (8 mice); n = cells, each cell from a new slice, and each experiment from > 3 mice; unpaired Student's t-tests; data are reported as the mean ± SD.